Chemistry–A European Journal
Research Article
doi.org/10.1002/chem.202402774
Chemistry Europe
European Chemical Societies Publishing
www.chemeurj.org

Tuning the Steric and Electronic Properties of Hemilabile NHC ligands for Gold(I/III) Catalyzed Oxyarylation of Ethylene: A Computational Study

Gaetano Galdi[a] and Chiara Costabile*[a]

Mechanistic studies on 1,2-oxyarylation of ethylene promoted by gold catalysts bearing hemilabile N-Heterocyclic Carbene (NHC^X) ligands were conducted by DFT calculations, exploring the whole catalytic cycle. After highest energy transition state (TS) barriers were located for NHC^N gold catalyst, and experimental results with different iodoarenes and alcohols rationalized, the study was extended to modified NHC^X catalysts, to observe how electronic and steric effects could affect the rate determining step TS. Electronic effects were investigated on NHC^X (X = H, N, O, P, and S), whereas steric effects emerged when comparing catalysts with different N–R groups (R = Dipp, Mes, tBu and Me). Finally, we suggest a different catalyst design based on *N*-aryl *N*-*o*-donor-aryl NHC, with different donors and NHC backbones to search for better performing systems.

Introduction

Over the past twenty years, gold emerged as a leading metal in the organic synthesis.[1] Among the most relevant properties of gold, the high functional group tolerance, environmental friendly nature, and orthogonal reactivity with respect to many transition metals increased the great successes gained in catalysis. The two possible oxidation states of gold species, Au(I) and Au(III), made this metal a versatile catalyst involved in the activation of multiple carbon-carbon bonds, as well as in oxidation and coupling reactions.[2]

Oxyarylation of alkenes represents a powerful tool to build new organic scaffolds from simple and cheap substrates.[3] The recent synthesis of new gold catalysts able to stabilize Au(III) species[4] includes the pioneering work of Bourissou on diphosphine gold complexes (**1** of Scheme 1),[5,6] followed by the development of chelating (P,N) Me-DalPhos gold complex (**2**),[7–9] along with their chiral analogous,[10,11] and by the synthesis of bipyridyl gold catalysts by Russell and coworkers (**3**).[12] After the introduction of the first free oxidant gold catalyst bearing the classical Ipr *N*-Heterocyclic ligand (NHC), able to promote C–O coupling,[13,14] Ribas and coworkers developed an hemilabile MIC^N Au catalyst (**4**) active in the arylation-lactonization of γ-alkenoic acids.[15] Shi, in 2020, reported on the 1,2-oxyarylation of alkenes in the presence of Me-DalPhos gold complexes, introducing an easy one-pot strategy for alkene difunctionalization.[16] Finally, Russell very recently introduced a gold catalyst, bearing a chelating (C^N) N-Heterocyclic Carbene (NHC) ligand, able to promote for the first time 1,2 oxyarylations of ethylene and propylene in the absence of exogenous oxidants (**5**).[17] Meanwhile, complex **5** was shown to be active in aryl C–H arylations by Zhang, Szostak and coworkers.[18]

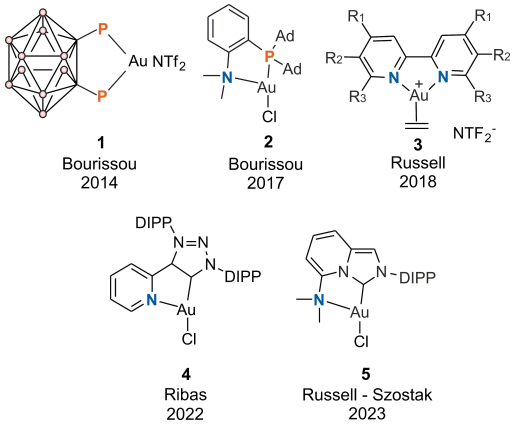

Scheme 1. Au-based complexes with ligands able to stabilize A(I)/Au(III) species.

Since the first synthesis and isolation of a stable carbene by Arduengo,[19] NHCs burst into the coordination chemistry with a leading role in catalysis complexes for their easy tunable steric and electronic properties[20] performing a determinant duty in gold catalysis.[21] The modification of the NHC architecture can play a fundamental role in the stabilization of Au(I)/Au(III) species, as also highlighted in recent experimental and computational studies.[11,13,14,17,18,22]

1,2-oxyarylation of ethylene or propylene in the absence of a strong external oxidant can be performed with a I-aryl and an alcohol (Scheme 2), involving both Au(I) and Au(III) species in the catalytic cycle.[7,16,17,23] Indeed, several computational studies

[a] G. Galdi, C. Costabile
Department of Chemistry and Biology "A.Zambelli", University of Salerno, Via Giovanni Paolo II, 132, 84084 Fisciano, SA, Italy
E-mail: ccostabile@unisa.it

Supporting information for this article is available on the WWW under https://doi.org/10.1002/chem.202402774

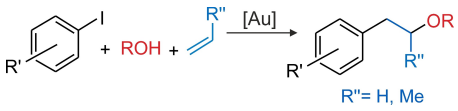

Scheme 2. 1,2-oxyarylation of ethylene or propylene.

have been recently focused on the energy barriers of the aryl iodide oxidative addition that represents a key step not only for 1,2-oxyarylation of alkenes, but also for a large class of reactions involving Au catalyzed arylations.[2f,5,8,17,23,24]

For this reason, the catalyst activity for 1,2-oxyarylation was mainly attributed to the ability of the ligand to lower the energy barrier of the oxidative addition, stabilizing the formation of the Au(III) intermediate (Scheme 3).[17] Bourissou and coworkers investigated the attack of the alcohol to the C=C double bond, in the framework of the cyclization of alkenols involved in oxyarylation reaction. Nevertheless, in this DFT mechanistic study, the preliminary oxidative addition was not investigated.[23] To the best of our knowledge, no computational study on the whole catalytic cycle relative to 1,2-oxyarylation reaction was performed yet.

Herein, a DFT study on the entire catalytic cycle of 1,2-oxyarylation in the presence of hemilabile NHC^N–Au catalyst **5** is afforded with the intent to identify the rate determining steps and design NHC ligands suitable to lower the energy barriers. As first step, experimental yields reported by Russell on varying the iodoarene and the alcohol were rationalized. The computational study was then extended to **5**-type complexes with different donors on NHC ligand (Scheme 4), to investigate electronic interactions with the metal, and with different *N*-substituents on the other side of NHC to evaluate the steric impact on the catalytic pocket. In the attempt to conceive more active complexes, the DFT study was further enlarged to saturated and unsaturated NHC ligands bearing *N*-mesityl *N'*-aryl substituents with an ortho donor group (**6**-type complexes in Scheme 4).

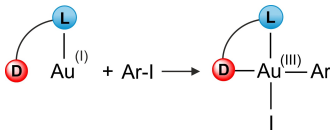

Scheme 3. Oxidative addition of an aryl iodide to Au(I).

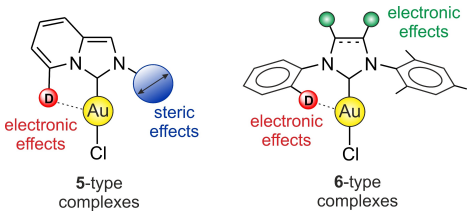

Scheme 4. Schematic description of 5-type gold complexes and N-mesityl N-aryl NHC (6-type) complexes.

Results and Discussion

DFT Mechanistic Studies on Catalyst 5

The catalytic cycle relative to 1,2-oxyarylation of ethylene, is reported in Scheme 5. NHC-gold chloride complex **a**, in the presence of silver antimonate, gives the Au(I) catalytic active species **b**. After exchange of antimonate with the iodoarene the Au(I) intermediate **c** can undergo oxidative addition, generating Au(III) intermediate **d**.

The precipitation of AgI leads to the formation of ethylene coordinated intermediate **e**, that can go through nucleophilic attack from the alcohol giving the Au(III) intermediate **f**. The reductive elimination restores Au(I) species **b** delivering the desired product.

The experimental driving force in the oxidative addition of iodoarene is the presence of $AgSbF_6$, that is added in stoichiometric excess with respect to the iodoarene and plays a double role in precipitating AgCl to give the active species and AgI during the catalytic cycle.[17,23]

The free energy profile of the described catalytic cycle in the presence of complex **5** is reported in Figure 1. All reported energies were calculated at the M06/6311++G(d,p)/Def2TVZPP level of theory with Grimme's dispersion correction in *ortho*-dichlorobenzene (*o*-DCB) according to the procedure reported in the computational details of SI. In this preliminary study we choose to investigate 1,2-oxyarylation of ethylene with iodobenzene and ethanol. All energies were calculated with respect to species **5N_b**. As depicted in Figure 1, the transition state (TS) involving the exchange of antimonate with the iodobenzene ($[\mathbf{5N\_b–c}]^{\neq}$) was calculated to be only −0.2 kcal/mol.

Although free energy of $[\mathbf{5N\_b–c}]^{\neq}$ is lower than the preceding minimum energy intermediate **5N_b**, this species is technically a TS, and leads to the quite stable intermediate **5N_**

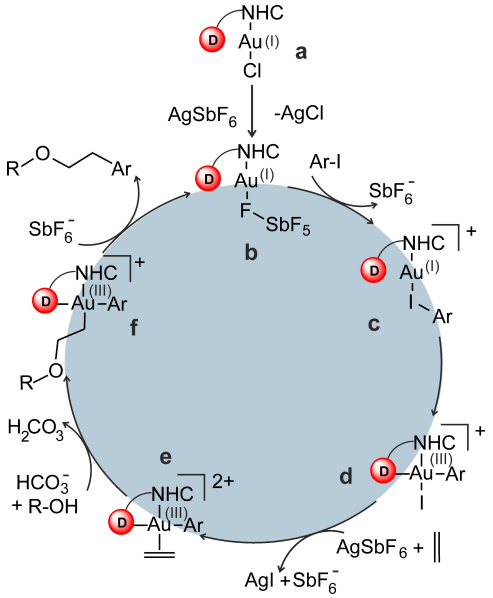

Scheme 5. Catalytic cycle of 1,2 oxyarylation of ethylene.

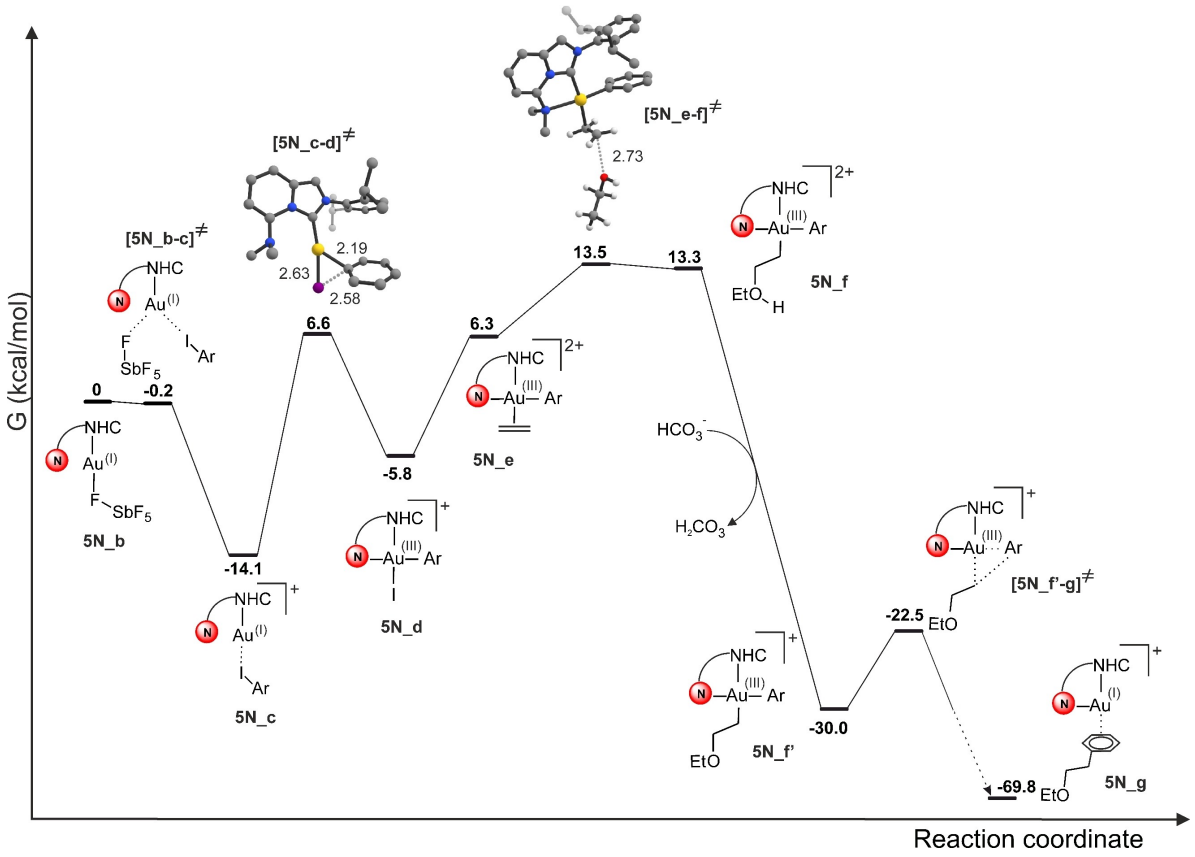

Figure 1. Free energy profile in *o*-DCB of 1,2-oxyarylation of ethylene with iodobenzene and ethanol. For the sake of clarity all intermediates and TS were schematized except for oxidative addition TS **[5N_c–d]**$^{\neq}$ and alcohol attack to ethylene TS **[5N_e–f]**$^{\neq}$, where optimized geometries are depicted. Energies are in kcal/mol, bond length are in Å.

c (−14.1 kcal/mol). The oxidative addition of iodobenzene shows to be more expensive with the TS **[5N_c–d]**$^{\neq}$ presenting a free energy of 6.6 kcal/mol. The relative ΔΔG barrier **c**→**[c–d]**$^{\neq}$ of 20.7 kcal/mol is coherent with the barriers reported in literature for this step[17] (although in ref.[17] *N*-2,6-diisopropyl phenyl was modeled by an *N*-2,6-dimethylphenyl group, that does not represent a trivial approximation, as it will be shown in the Steric Effects section). The coordination of ethylene starting from Au(III) intermediate **5N_d** is driven by the precipitation of AgI and gives intermediate **5N_e** with higher free energy (6.3 kcal/mol), mainly due to the double positive charge of this intermediate. The nucleophilic attack on ethylene by ethanol (**[5N_e–f]**$^{\neq}$) exhibits a TS free energy of 13.5 kcal/mol, that is the highest energy of the overall pathway. Intermediate **5N_f** then falls without barrier to the corresponding species **5N_f'** (ΔG = −30.0 kcal/mol), after deprotonation with bicarbonate (Figure S17). Last step is the reductive elimination of the product that occurs with a low energy (ΔG = −22.5 kcal/mol) and gives the (2-ethoxyethyl)benzene coordinated species **5N_g** at ΔG = −69.8 kcal/mol. Reductive elimination energy barrier (ΔΔG = 7.5 kcal/mol) is much lower than the Csp^2-Csp^3 reductive elimination barrier reported by Datta for a diphosphine gold complex (ΔΔH = 18 kcal/mol)[25] and slightly lower than recently one reported by Xing and Chen[26] (ΔΔG = 10.7 kcal/mol) for an alkene 1,2 oxyarylation in the presence of a Me-Dalphos gold complex. Nevertheless, differently from ref. [26] the absolute energy that we found for the reductive elimination is much lower than for nucleophilic alcohol attack TS, due to the overall catalytic system. Indeed, as for the alkene 1,2 oxyarylation energy profile reported in ref. [26], the nucleophilic alcohol attack is assisted by the triflate (silver salt is AgOTf), and the intermediate and TS involved in the nucleophilic alcohol attack present a +1 charge, as those involved in the reductive elimination. On the contrary, we describe a catalytic system where the reaction is conducted in the presence of $AgSbF_6$ with SbF_6^- far from the metal during the nucleophilic alcohol attack. Consequently, this step involves +2 charged species (Figure 1).

Considering the reported energy profile, the meaningful energy TSs for 1,2-oxyarylation of ethylene revealed to be the oxidative addition and the nucleophilic alcohol attack. For this specific reaction the nucleophilic alcohol attack surprisingly emerged as the rate determining step. Although much attention was dedicated in the literature to oxidative addition, suggested as key step not only in oxyarylations[17] but also in other coupling reactions,[8,15,24,26] only few studies were reported on the alcohol attack and, with the exception of ref,[26] investigated the regioselectivity in intramolecular ring closing.[7,23]

In light of this observations we enlarged the investigations to other aryl iodides experimentally explored by Russell, with electron-withdrawing groups (as 4-fluoroiodobenzene and 4-iodonitrobenzene) and electron-donating groups (as 4-iodoaniline).[17] Computational outcomes are resumed in Table 1 (energy profiles are reported in Figure S4) and compared with the experimental isolated yield reported in the literature. For a homogeneous comparison, all experimental yields, reported in Table 1, refer to oxyarylation with butanol, whereas the modeled alcohol is ethanol. As reported by Russell, aryl iodides with strong electron-withdrawing groups as NO_2 and fluorine lead to lower yields. According to DFT studies, this is an outcome of the increase of the energy barrier for the alcohol attack to ethylene ($\Delta G = 16.2$ for NO_2 and 14.7 for F) with respect to iodobenzene ($\Delta G = 13.5$). Indeed, the nucleophilic attack to ethylene occurs on a coordination intermediate with two positive charges, which is destabilized by σ bound aryls with para electron-withdrawing substituents (see **5N_e** free energies in Table 1). The corresponding TS energies are destabilized as well for the same reasons.

When aryl iodide bears a *p*-bromine barriers are comparable to iodobenzene. The slight decrease of yield is possibly due in this case to **5N_c** minimum coordination energy where Br coordination starts to be competitive with I coordination. This effect becomes self-evident for aryl iodide with *p*-amino substituent, where the coordination of $-NH_2$ leads to a much stable intermediate behaving as a catalyst poison (Figure S4).

Finally, when alcohol attack **[e–f]**$^{\neq}$ was calculated with methanol instead of ethanol, an increase of energy was revealed ($\Delta G = 14.6$ kcal/mol). In agreement with lower experimental yields (49%)[17] oxyarylation with methanol is less favored, although is worth noting that the yield drop could be also related to experimental temperature conditions (75 °C is over the methanol boiling point and would certainly lower the alcohol concentration in solution).

Tuning Steric and Electronic Properties of Catalyst 5

Once highest barriers for 1,2 oxyarylation of ethylene were located, we introduced electronic and steric modifications of the NHC ligand, to investigate how they would affect the rate of the reaction.

Electronic effects

Starting from **5** catalyst architecture, we calculated the energy profiles from **b** to **g** on varying the donor (Figure S1). Free energies of oxidative addition TS (**[c–d]**$^{\neq}$), alcohol attack TS (**[e–f]**$^{\neq}$) as well as reductive elimination TS (**[f′-g]**$^{\neq}$) for **5**-type complexes have been sketched in Table 2.

The calculated energies were compared with those obtained for Russell catalyst (**5N**) and reported in Table 2. In the absence of a donor (**5H**), the barrier for oxidative addition ($\Delta G = 13.2$) is increased of 7.6 kcal/mol with respect to **5N**, coherently with that reported in ref[17] ($\Delta\Delta G = +3.7$). Nevertheless, according to our results, the greatest disadvantage of the donor elimination lies in the increase of the alcohol attack energy (for **5H_[e–f]**$^{\neq}$ $\Delta G = 32.4$ kcal/mol).

Slightly higher oxidative addition TS free energies were observed when $-N(CH_3)_2$ group is replaced by $-OCH_3$, $-P(CH_3)_2$, and $-SCH_3$. As for alcohol attack a different trend was observed: TS energy turned out to be very high for **5O** (25.3 kcal/mol) and surprisingly low for **5P** (2.9 kcal/mol).

To rationalize **[e–f]**$^{\neq}$ energy differences Natural Bond Orbital (NBO) analysis was performed on **[e–f]**$^{\neq}$ geometries. According to the obtained results, we observed that, the latter TS free energies were inversely proportional to the electron donating ability of the heteroatom donor (Table 2). The electron donation has been quantified as the overall interaction energy involved in the electron donation from the lone pair located on the heteroatom donor (LP_D) to an empty molecular orbital of the Au-aryl bond ($MO^*_{Au\text{-}C(aryl)}$). The strong linear correlation is shown in Figure 2.

Table 1. Free energy of **[5N_c–d]**$^{\neq}$ and **[5N_e–f]**$^{\neq}$ TSs and of **5N_e** and **5N_c** intermediates on varying the aryl iodide. Zero free energy is represented by minimum energy intermediate **b** of the catalytic cycle. Energies are in kcal/mol.

Iodoarene	ΔG [5N_c–d]$^{\neq}$	ΔG [5N_e–f]$^{\neq}$	ΔG 5N_e	ΔG 5N_c[a]	Yield %[b]
	6.6	13.5	6.3	(I) −14.1	85
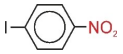	6.2	16.2	9.0	(I) −12.1 (NO_2) −4.3	11
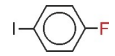	7.4	14.7	7.4	(I) −13.6 (F) +7.0	71
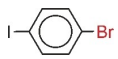	6.3	13.3	6.5	(I) −13.8 (Br) −9.3	71
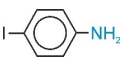	5.7	14.1	5.4	(I) −14.2 (NH_2) −18.3	traces

[a] Minimum coordination iodoaryl intermediate energies presenting an Au–I interaction (I) or an Au–X (X=NO_2, F, Br, NH_2) interaction (X). [b] Isolated yields reported in ref.[17] for the 1,2-oxyarylation of ethylene with the corresponding iodoaryl and butanol.

Table 2. Free energies in kcal/mol of oxidative addition TS ([**c–d**]$^{\neq}$) and alcohol attack TS ([**e–f**]$^{\neq}$) for **5**-type complexes sketched below. Calculated geometries are reported in Figure S3. Zero free energy is represented by the corresponding minimum energy intermediate **b** of the catalytic cycle. Electron donation from the valence lone pair (LP) located on the heteroatom donor to an empty molecular orbital (MO*) of the Au-aryl bond from NBO analysis is expressed as stabilizing interaction energy in kcal/mol.

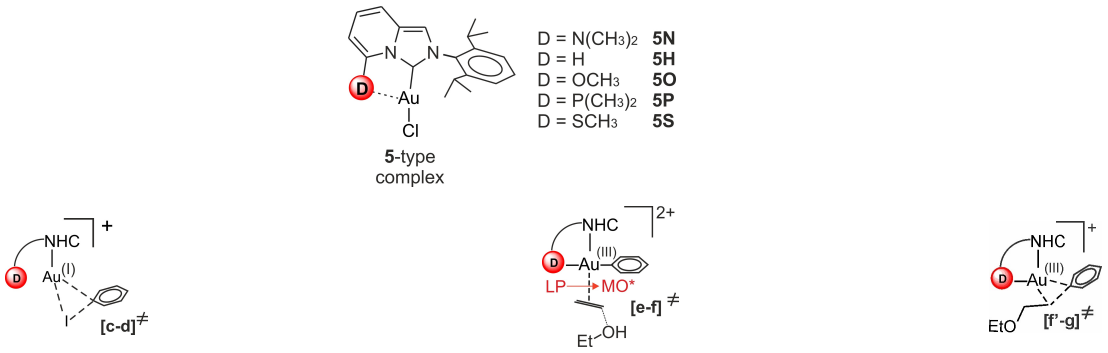

5-type	ΔG[c-d]$^{\neq}$	ΔG[e-f]$^{\neq}$	$LP_D \rightarrow MO^*_{Au\text{-}C(aryl)}$	ΔG[f'-g]$^{\neq}$
5N	6.6	13.5	44.1	−22.5
5H	13.2	32.4	-	−15.1
5O	10.6	25.3	14.4	−20.5
5P	7.8	2.9	100.7	−19.2
5S	7.7	13.0	50.0	−21.0

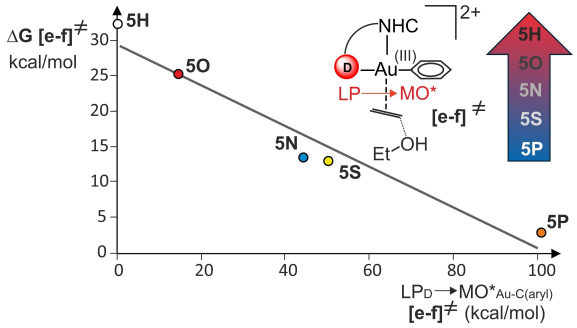

Figure 2. Correlation between [**e–f**]$^{\neq}$ free energies and electron donation from lone pair of the donor pendant arm (LP_D) to the antibonding molecular orbital (MO*) of the gold-C_{aryl} bond. As for the linear regression $R^2 = 0.9446$.

As for reductive elimination, even changing the donor [**f'-g**]$^{\neq}$ TS still retains a low energy (Table 2). Nevertheless, TS barriers with respect to the previous minimum energy intermediates strongly depend on the donor nature (ΔΔG = 0.5, 1.5, 7.5, 9.4, and 20.2 kcal/mol for D=H, O, N, S, and P, respectively, Figure S1). It is worth noting that the free energy barrier of 20.2 kcal/mol found for the NHC^P gold catalyst is very close to the enthalpy barrier calculated by Datta and coworkers for a Csp^2–Csp^3 reductive elimination in the presence of a gold (III) system bearing two PH_3 (18.0 kcal/mol).[25]

In summary, considering the high TS energies calculated for the alcohol attack (except for **5P**, where oxidative addition TS energy overcome alcohol attack), the performances of the analyzed complexes should decrease in the order **5P** > **5S** > **5N** > **5O** > **5H**. Indeed, a higher electron donation would lead to a higher stabilization of the alcohol attack TS characterized by +2 charge, whereas the rest of the catalytic cycle involves 0 or +1 charged species.

The reluctance of oxygen as a pendant donor functionality to coordinate gold even in high oxidation state is testified also by recent experimental studies.[27]

Steric effects

An attempt to predict catalyst efficiency on varying the dimension of the catalytic pocket was performed by calculating [**c–d**]$^{\neq}$ and [**e–f**]$^{\neq}$ TS with different *N*-substituents. Once again, the alcohol attack energy barrier [**e–f**]$^{\neq}$ represents the highest step to be overtaken and follows the trend ^{t}Bu > Dipp > Me > Mes (Table 3, Figure S6). Nevertheless, it is worth noting that oxidative addition barrier follows [**c–d**]$^{\neq}$ the same trend. The energies reported in Table 3 have been compared with main geometrical parameters (angle θ and dihedral angle ϕ in Table 3) of [**e–f**]$^{\neq}$ TS and with the corresponding NHC percent buried volume (%V_{Bur}) of the starting complexes. %V_{Bur} is defined as the fraction of the total volume of a sphere centered on the metal occupied by a given ligand and is a parameter that quantifies the steric hindrance of ligands.[28] To complete the analysis, topographic steric maps were achieved by using the program downloadable from the SambVca web server[29] and depicted in Figure 3 (see computational detail in SI for used parameters). According to the located [**e–f**]$^{\neq}$ TS geometries, the highest [**e–f**]$^{\neq}$ energy barrier for **5N_^{t}Bu** can be ascribed to the high steric hindrance of ^{t}Bu group, also testified by the %V_{Bur} value. The *tert*-butyl distorts the [**e–f**]$^{\neq}$ geometry enlarging the C_{NHC}-Au-C_{aryl} angle to 99° and twisting the dihedral ϕ angle, deviating from the ideal square planar structure. A similar, but minor effect can be observed for **5N (Dipp)**, even if, as shown in topographic maps (Figure 3), the

Table 3. Free energies in kcal/mol of oxidative addition TS ([**c–d**]$^{\neq}$) and alcohol attack TS ([**e–f**]$^{\neq}$) for **5**-type complexes on varying the bulkiness and the nature of the *N*-subtituent. Geometries are reported in Figure S7. Zero free energy is represented by the corresponding minimum energy intermediate **b** of the catalytic cycle.

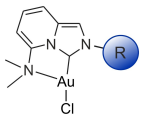

5-type complex

R = Dipp **5N (Dipp)**
R = Mes **5N_Mes**
R = Me **5N_Me**
R = ᵗBu **5N_ᵗBu**

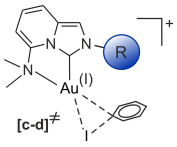

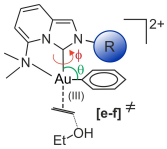

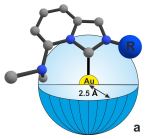

complex	[**c–d**]$^{\neq}$	[**e–f**]$^{\neq}$	θ	ϕ	%V_{Bur}
5N(Dipp)	6.6	13.5	96.6	−4.3	38.5
5N_Mes	5.1	10.2	95.3	5.7	37.2
5N_Me	8.1	12.7	94.3	−0.7	36.0
5N_ᵗBu	11.4	18.6	99.1	−16.5	40.4

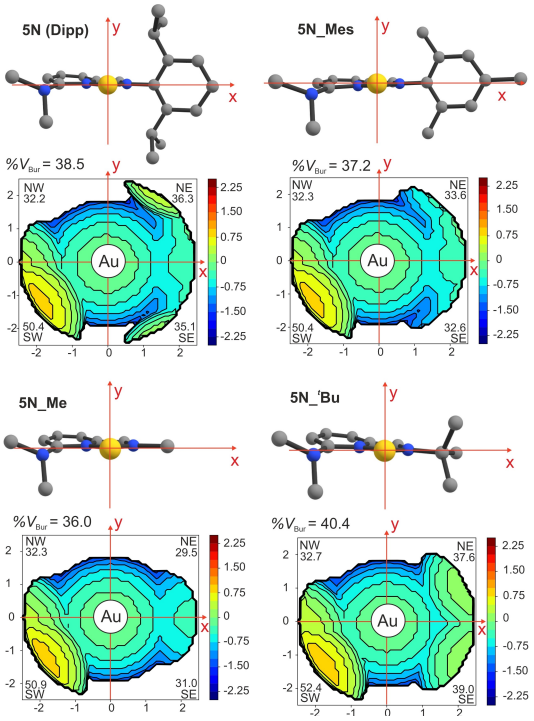

Figure 3. Topographic steric maps of **5**-type complexes. The isocontour curves of steric maps are in Å. The maps were constructed starting from the NHC-AuCl structures of complexes optimized by DFT calculations. The complexes are oriented according to the structure on the top of the map. Overall %V_{Bur} and %V_{Bur} representative of each single quadrant are reported for each map.

steric hindrance of the Dipp is located more external with respect to the catalytic pocket. Different %V_{Bur} of **5N (Dipp)**, reported by Szostak[18] is due to the use of different setting parameters.

Surprisingly, [**e–f**]$^{\neq}$ TS energy for **5N_Mes** is lower than **5N_Me**. Possibly responsible for this results are, π-π stacking interactions observed in the [**e–f**]$^{\neq}$ TS geometries when R is an aryl group (Figure 4).

In conclusion, lowest barrier observed in **5N_Mes** is the result of favorable a π-π stacking interaction associated with a contained steric bulkiness.

New Catalyst Design

Catalyst **5** has the advantage of a constrained geometry where the donor group is close to the metal forming a five ring. Although electron donation stabilizes Au(III) species, Au(I) usually assume a linear geometry with only two occupied coordinative position. On the contrary, NHCs with a fluxional donor could, in principle, own all desirable properties: the ability to coordinate the donor in Au(III) square planar structures and to remove it in linear Au(I) structures. In this framework, DFT calculation were run on NHC gold complexes reported in Table 4. NHC ligands with *N*-aryl substituents represent a class of ligand widely used for the synthesis of metal complexes. For the reported computational study, we choose to first investigate complexes with saturated NHC bearing *N*-Mes group, calculated to be the ideal ancillary group on **5**-type complexes, and *N'*-aryl group with an ortho donor substituent (**6**-type complexes in Table 4). Saturated NHCs have, in addition, the advantage that a substitution on backbone easily leads to chiral complexes that can be useful for enantioselective catalysis.[30] The investigated complexes, or modified analogous, could be experimentally achievable. As for **6P** and **6S**, similar or identical NHC ligands were already synthetized and reported in the literature on different metals.[31,32] As for **6N**, NHC gold catalysts with *N*-Mes, *N'*-ethylene amino substituents has been obtained.[33] Several examples of gold complexes with NHC bearing oxygen donors have been also reported.[27,34]

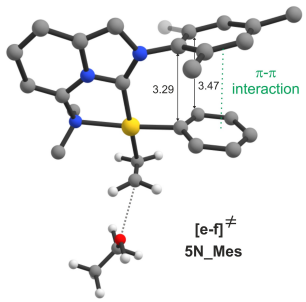

Figure 4. Minimum energy structure of **[e–f]**$^{\neq}$ TS for **5N_Mes**. Distances are in Å.

According to free energies of **[c–d]**$^{\neq}$ and **[e–f]**$^{\neq}$ TS of Table 4, complexes with NHC bearing a phosphine donor should be more efficient (energy profiles are sketched in Figure S8). As already observed for **5**-type catalysts, **6P** presents a **[e–f]**$^{\neq}$ TS energy significantly lower with respect to its analogous with **6N**, **6O** and **6S**. Indeed, whereas for the latter **[e–f]**$^{\neq}$ TSs represent the rate determining step and increase in the order **6N** < **6S** < **6O**, for **6P** the oxidative addition exhibits the highest TS energy. The low **[e–f]**$^{\neq}$ TS energy for **6P** can be rationalized by the significantly higher donor ability of phosphorus ($LP_D \rightarrow MO^*_{Au\text{-}C(aryl)}$ of 120 kcal/mol) with respect to other heteroatoms, reflected also in the lower Au positive charge. Despite the better donor ability of sulfur ($LP_D \rightarrow MO^*_{Au\text{-}C(aryl)}$ of 57.5 kcal/mol) compared to nitrogen, **6S** presents slightly higher **[e–f]**$^{\neq}$ TS energy, as a possibly effect of the ligand flexibility. Indeed, the higher ψ angle (Table 4) observed for **6S** possibly results in an overall lower stabilization of the TS.

Being **6P** far the most promising designed catalyst, TS energies were calculated also for diphenyl (**6PPh**) and diadamantyl (**6PAd**) phosphine substituted NHC. Both NHC ligands were already reported in the literature.[31] **[e–f]**$^{\neq}$ TS free energies significantly increase in the order **6P** < **6PPh** < **6PAd**. This trend is possibly related to the growth of the steric hindrance that closes the catalytic pocket (%V_{Bur} is 46.7, 49.2 and 50.9 for **6P_[e–f]**$^{\neq}$, **6PPh_[e–f]**$^{\neq}$ and **6PAd_[e–f]**$^{\neq}$, respectively. See SI for energy profiles, Figure S10 and topographic maps, Figure S14).

Nevertheless, **[c–d]**$^{\neq}$, that is the highest energy TS for **6P** and **6PPh**, do not show the same trend. In Table 5 the main parameters relative to **[c–d]**$^{\neq}$ geometries for phosphine donors have been collected. From NBO analysis no electronic factors, related to the donor interaction with gold able to rationalize the trend of oxidative addition energies, were found.

The lower free energy observed for **6PPh** complex can be ascribed to an electrostatic attractive interaction between the electron rich negative phenyl group of the donor and the ortho methyl group of mesityl (Figure 5. For electrostatic maps see also Figure S16). On the contrary, as for **6P** and **6PAd** the ortho methyl group of mesityl faces a methyl or an adamantyl group giving a repulsive electrostatic interaction.

Finally, the effect on TS energies of different backbones have been evaluated by replacing on **6N** an unsaturated backbone (**i6N**) and a fluorine substituted unsaturated backbone (**i6N_F**). The overall outcome can be summarized as an increase of the rate determining step **[e-f]**$^{\neq}$ TS free energy (**6N** < **i6N** < **i6N_F**), already visible in the previews olefin coordi-

Table 4. Free energies in kcal/mol of oxidative addition TS (**[c–d]**$^{\neq}$) and alcohol attack TS (**[e–f]**$^{\neq}$) for complexes sketched below. Geometries are reported in Figure S9, S11 and S13. Zero free energy is represented by the corresponding minimum energy intermediate **b** of the catalytic cycle. Electron donation from the valence lone pair (LP) located on the heteroatom donor to an empty molecular orbital (MO*) of the Au-aryl bond from NBO analysis is expressed

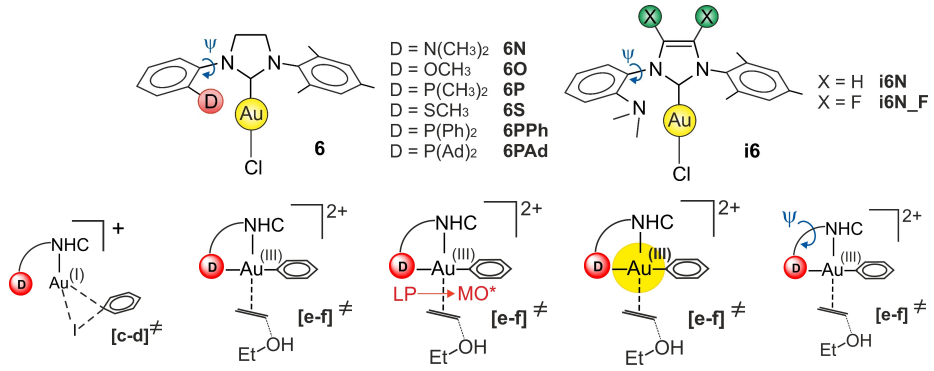

	$\Delta G[c\text{-}d]^{\neq}$	$\Delta G[e\text{-}f]^{\neq}$	$LP_D \rightarrow MO^*_{Au\text{-}C(aryl)}$	Au charge	Ψ [e-f] $^{\neq}$	$\%V_{Bur}$
6 N	7.1	11.4	40.1	0.867	−39.3	46.8
6O	11.0	22.0	27.8	0.880	−38.0	43.3
6P	7.8	−0.65	119.8	0.719	−41.2	46.7
6S	10.2	11.8	57.5	0.756	−41.5	45.6
6PPh	5.9	2.4	130.7	0.713	−37.6	49.2
6PAd	8.7	10.6	76.6	0.711	−39.5	50.9
i6N	7.5	13.2	42.0	0.866	−42.9	45.8
i6N_F	8.2	15.8	37.0	0.865	−43.4	45.7

Table 5. Oxidative addition free energies $\Delta G[c\text{–}d]^{\neq}$ of **6P**, **6PPh** and **6PAd** compared to main electronic and geometrical parameters (P–Au distances, overall P→Au donation and Au→P backdonation from NBO analysis, Au charge, Mayer bond order[35]).

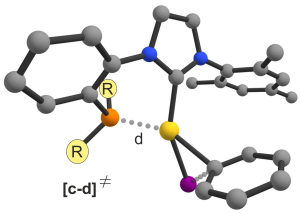

complex	ΔG [c-d]≠	d (P–Au)	P→Au[a] Au→P	Au charge	Mayer Bond Order (P–Au)
6P	7.8	2.45	1547	0.32	0.114
6PPh	5.9	2.48	1045	0.32	0.453
6PAd	8.7	2.47	687	0.34	0.712

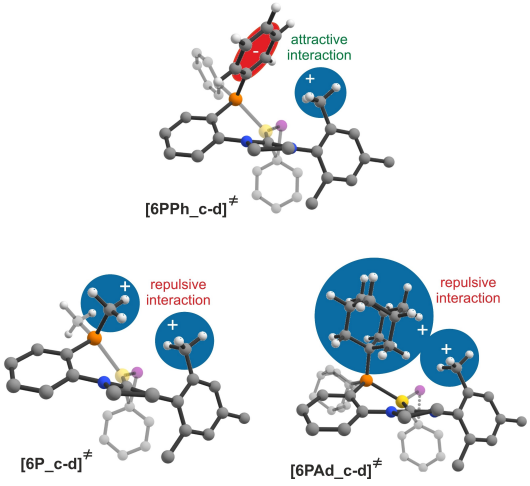

Figure 5. Electrostatic interactions for 6PPh_[c-d]≠, 6 P_[c-d]≠, and 6PAd_[c-d]≠.

nation minimum energy intermediate e (ΔG = 4.2, 5.0 and 9.0 kcal/mol for intermediate **6N_e**, **i6N_e** and **i6N_F_e** respectively, Table S6 and Figure S12). The observed trend is mainly related to the decrease of σ donation ability going from the saturated to the fluorine substituted NHC, that rises the σ donation of ethylene, as testified by the decrease of C=C Mayer bond order[35] (ethylene MBO = 1.63, 1.60 and 1.56 for intermediate **6N_e**, **i6N_e** and **i6N_F_e** respectively, Table S7). It is not surprising that the lack of NHC σ donation ability destabilizes intermediates and TSs of high charged species (+2) as e and **[e-f]**≠.

In summary, **6**-type gold complexes are a promising class of catalysts for 1,2-oxyarylation of ethylene. Calculated energy barriers for rate determining step TS are comparable or lower than those of **5**-type catalysts. Phosphorus has been confirmed as best donor also for this class complexes, being able to stabilize high gold oxidation states. The most promising designed complex, **6PPh**, showed as highest TS energy step, the oxidative addition, with a ΔG of only 5.9 kcal/mol.

Conclusions

The catalytic cycle of 1,2-oxyarylation of ethylene in the presence of hemilabile NHC^N gold catalyst (**5**) was fully explored by DFT studies. For this catalyst, alcohol attack to ethylene emerged as rate determining step, followed by the oxidative addition, that exhibits a lower free energy TS. According to the calculated TSs, the decrease of efficiency of **5** toward aryl iodide with para electron withdrawing groups depends on the increase of the alcohol attack barrier, whereas the drop in case of strong electron donating groups (e.g. $-NH_2$) lies in the strong coordination energy of the *p*-group in place of the iodine. In the attempt to design more efficient catalysts, energy profiles for **5**-type complexes on varying the donor were calculated. Soft donors (P and S) would lower the alcohol attack barrier, as a result of a more efficient electron donation in empty molecular orbitals of the Au-C_{aryl} bond. This effect showed to be strongly meaningful for **5P** complex, where oxidative addition turned to be the rate determining step. Variation of the nature of the ancillary *N*-substituent, on the other side of the NHC, leads to conclude that high steric hindrance would be not desirable, however the substituent should preferably be an aryl group. Among the considered substituents, **5**-type catalyst with *N*-mesityl exhibited lowest TS energies.

Finally, an alternative gold catalyst architecture, bearing NHC ligands with *N*-mesityl *N'-o*-donor-substituted aryl groups (**6**-type complexes) has been proposed. By virtue of the greater σ donation character, saturated NHC ligands would lend higher efficiency to gold complexes with respect to unsaturated or electron withdrawing backbone substituted NHC ligands. In addition, saturated backbone gives the opportunity of easily introduce chiral ligands. According to our investigations, phosphorus still revealed as best donor. Lowest barriers were shown in the presence of **6PPh**, whose NHC ligand synthesis is already reported in the literature. Among all complexes considered in this computational study, **6PPh** appears as the most promising catalyst for 1,2-oxyarylation of ethylene.

More generally, in light of this computational study, the NHC^P combination revealed of high interest in designing gold catalyst ligands for 1,2-oxyarylation of alkene.

Acknowledgements

This work received financial support from the University of Salerno (FARB) and from PRIN 2022 (Progetti di Rilevante Interesse Nazionale) Grant 2022ZJSCW3 from MUR, Italy. We thank Dr. Assunta D'Amato and Prof. Fabia Grisi for useful discussions. Open Access publishing facilitated by Università degli Studi di Salerno, as part of the Wiley - CRUI-CARE agreement.

Conflict of Interests

The authors declare no conflict of interest.

Data Availability Statement

The data that support the findings of this study are available in the supplementary material of this article.

Keywords: Gold · NHC · Oxyarylation · DFT

[1] a) Z. Li, C. Brouwer, C. He, *Chem. Rev.* **2008**, *108*, 3239; b) A. S. K. Hashmi, D. F. Toste, *Modern Gold Catalyzed Synthesis*, Wiley-VCH, Weinheim, **2012**; c) L. M. Slaughter, Ed., *Homogeneous Gold Catalysis*, Springer, Cham Heidelberg, **2015**; d) D. Pflästerer, A. S. K. Hashmi, *Chem. Soc. Rev.* **2016**, *45*, 1331–1367; e) C. C. Chintawar, A. K. Yadav, A. Kumar, S. P. Sancheti, N. T. Patil, *Chem. Rev.* **2021**, *121*, 8478; f) D. Campeau, D. F. León Rayo, A. Mansour, K. Muratov, F. Gagosz, *Chem. Rev.* **2021**, *121*, 8756.

[2] a) M. N. Hopkinson, A. D. Gee, V. Gouverneur, *Chem. Eur. J.* **2011**, *17*, 8248; b) L. T. Ball, G. C. Lloyd-Jones, C. A. Russell, *J. Am. Chem. Soc.* **2014**, *136*, 254–264; c) S. Kramer, *Chem. Eur. J.* **2016**, *22*, 15584; d) I. Stylianakis, A. Kolocouris, *Catalysts* **2023**, *13*, 921; e) Z. Zheng, X. Ma, X. Cheng, K. Zhao, K. Gutman, T. Li, L. Zhang, *Chem. Rev.* **2021**, *121*, 8979; f) A. Nijamudheen, A. Datta, *Chem. Eur. J.* **2020**, *26*, 1442.

[3] a) A. D. Melhado, W. E. Jr. Brenzovich, A. D. Lackner, F. D. Toste, *J. Am. Chem. Soc.* **2010**, *132*, 8885; b) L. T. Ball, M. Green, G. C. Lloyd-Jones, C. A. Russell, *Org. Lett.* **2010**, *12*, 4724; c) G. Zhang, L. Cui, Y. Wang, L. Zhang, *J. Am. Chem. Soc.* **2010**, *132* (5), 1474.

[4] a) M. Joost, A. Amgoune, D. Bourissou, *Angew. Chem. Int. Ed.* **2015**, *54*, 15022; b) L. Rocchigiani, M. Bochmann, *Chem. Rev.* **2021**, *121*, 8364; c) V. W. Bhoyare, A. G. Tathe, A. Das, C. C. Chintawar, N. T. Patil, *Chem. Soc. Rev.* **2021**, *50*, 10422; d) P. Font, H. Valdés, X. Ribas, *Angew. Chem. Int. Ed.* **2024**, *63*, e202405824.

[5] M. Joost, A. Zeineddine, L. Estévez, S. Mallet–Ladeira, K. Miqueu, A. Amgoune, D. Bourissou, *J. Am. Chem. Soc.* **2014**, *136*, 14654.

[6] M. Joost, L. Estévez, K. Miqueu, A. Amgoune, D. Bourissou, *Angew. Chem. Int. Ed.* **2015**, *54*, 5236.

[7] M. Rigoulet, O. Thillaye du Boullay, A. Amgoune, D. Bourissou, *Angew. Chem. Int. Ed.* **2020**, *59*, 16625.

[8] A. Zeineddine, L. Estévez, S. Mallet-Ladeira, K. Miqueu, A. Amgoune, D. Bourissou, *Nat. Commun.* **2017**, *8*, 565.

[9] a) C. C. Chintawar, A. K. Yadav, N. T. Patil, *Angew. Chem. Int. Ed.* **2020**, *59*, 11808; b) J. Rodriguez, A. Tabey, S. Mallet-Ladeira, D. Bourissou, *Chem. Sci.* **2021**, *12*, 7706; c) D. Vesseur, S. Li, S. Mallet-Ladeira, K. Miqueu, D. Bourissou, *J. Am. Chem. Soc.* **2024**, *146*, 11352.

[10] a) C. C. Chintawar, V. W. Bhoyare, M. V. Mane, N. T. Patil, *J. Am. Chem. Soc.* **2022**, *144*, 7089; b) X. Ye, C. Wang, S. Zhang, Q. Tang, L. Wojtas, M. Li, X. Shi, *Chem. Eur. J.* **2022**, *28*, e202201018.

[11] A. B. Gade, N. Urvashi, T. Patil, *Org. Chem. Front.* **2024**, *11*, 1858.

[12] a) M. J. Harper, C. J. Arthur, J. Crosby, E. J. Emmett, R. L. Falconer, A. J. Fensham-Smith, P. J. Gates, T. Leman, J. E. McGrady, J. F. Bower, C. A. Russell, *J. Am. Chem. Soc.* **2018**, *140*, 4440; b) J. A. Cadge, J. F. Bower, C. A. Russell, *Angew. Chem. Int. Ed.* **2021**, *60*, 24976.

[13] J. Serra, C. J. Whiteoak, F. Acuña-Parés, M. Font, J. M. Luis, J. Lloret-Fillol, X. Ribas, *J. Am. Chem. Soc.* **2015**, *137*, 13389.

[14] J. Serra, T. Parella, X. Ribas, *Chem. Sci.* **2017**, *8*, 946.

[15] P. Font, H. Valdés, G. Guisado-Barrios, X. Ribas, *Chem. Sci.* **2022**, *13*, 9351.

[16] S. Zhang, C. Wang, X. Ye, X. Shi, *Angew. Chem. Int. Ed.* **2020**, *59*, 20470.

[17] S. C. Scott, J. A. Cadge, G. K. Boden, J. F. Bower, C. A. Russell, *Angew. Chem. Int. Ed.* **2023**, *62*, e202301526.

[18] P. Gao, J. Xu, T. Zhou, Y. Liu, E. Bisz, B. Dziuk, R. Lalancette, R. Szostak, D. Zhang, M. Szostak, *Angew. Chem. Int. Ed.* **2023**, *62*, e202218427.

[19] A. J. I. Arduengo, R. L. Harlow, M. Kline, *J. Am. Chem. Soc.* **1991**, *113*, 361.

[20] a) H. Jacobsen, A. Correa, A. Poater, C. Costabile, L. Cavallo, *Coord. Chem. Rev.* **2009**, *253*, 687; b) S. Díez-González, N. Marion, S. P. Nolan, *Chem. Rev.* **2009**, *109*, 3612.

[21] N. Marion, S. P. Nolan, *Chem. Soc. Rev.* **2008**, *37*, 1776.

[22] a) E. Tomás-Mendivil, P. Y. Toullec, J. Borge, S. Conejero, V. Michelet, V. Cadierno, *ACS Catal.* **2013**, *3*, 3086; b) A. G. Nair, R. T. McBurney, M. R. D. Gatus, S. C. Binding, B. A. Messerle, *Inorg. Chem.* **2017**, *56*, 12067.

[23] M. Rigoulet, K. Miqueu, D. Bourissou, *Chem. – Eur J.* **2022**, *28*, e202202110.

[24] a) J. Rodriguez, A. Zeineddine, E. D. S. Carrizo, K. Miqueu, N. Saffon-Merceron, A. Amgoune, D. Bourissou, *Chem. Sci.* **2019**, *10*, 7183; b) J. Xu, X. Ma, C. Liu, D. Zhang, *J. Org. Chem.* **2022**, *87*, 4078; c) K. Muratov, E. Zaripov, M. V. Berezovski, F. Gagosz, *J. Am. Chem. Soc.* **2024**, *146*, 3660.

[25] A. Nijamudheen, S. Karmakar, A. Datta, *Chem. Eur. J.* **2014**, *20*, 14650.

[26] Y.-Y. Xing, D.-Z. Chen, *Comput. Theor.l Chem.* **2024**, *1233*, 114508.

[27] H. Freyr Jónsson, A. Orthaber, A. Fiksdahl, *Dalton Trans.* **2021**, *50*, 5128.

[28] a) R. Dorta, E. D. Stevens, N. M. Scott, C. Costabile, L. Cavallo, C. D. Hoff, S. P. Nolan, *J. Am. Chem. Soc.* **2005**, *127*, 2485; b) L. Cavallo, A. Correa, C. Costabile, H. Jacobsen, *J. Organomet. Chem.* **2005**, *690*, 5407.

[29] a) L. Falivene, R. Credendino, A. Poater, A. Petta, L. Serra, R. Oliva, V. Scarano, L. Cavallo, *Organometallics* **2016**, *35*, 2286; b) L. Falivene, Z. Cao, A. Petta, L. Serra, A. Poater, R. Oliva, V. Scarano, L. Cavallo, *Nat. Chem.* **2019**, *11*, 872.

[30] a) T. J. Seiders, D. W. Ward, R. H. Grubbs, *Org. Lett.* **2001**, *3*, 3225; b) C. Costabile, L. Cavallo, *J. Am. Chem. Soc.* **2004**, *126*, 9592; c) P.-A. Fournier, S. K. Collins, *Organometallics* **2007**, *26*, 2945; d) S. Tiede, A. Berger, D. Schlesiger, D. Rost, A. Lühl, S. Blechert, *Angew. Chem. Int. Ed.* **2010**, *49*, 3972; e) C. Costabile, A. Mariconda, L. Cavallo, P. Longo, V. Bertolasi, F. Ragone, F. Grisi, *Chem. Eur. J.* **2011**, *17*, 8618; f) Z. Szabo, M. Timari, R. Kassai, B. Szokol, A. C. Benyei, T. Gáti, A. Paczal, A. Kotschy, *Organometallics* **2020**, *39*, 3572; g) C. Costabile, S. Pragliola, F. Grisi, *Symmetry* **2022**, *14*, 1615; h) F. Tufano, F. Santulli, F. Grisi, M. Lamberti, *ChemCatChem* **2022**, *14*, e202200962.

[31] a) J. Zhong, J.-H. Xie, A.-E. Wang, W. Zhang, Q.-L. Zhou, *Synlett* **2006**, *2006*, 1193; b) C. A. Wheaton, J.-P. J. Bow, M. Stradiotto, *Organometallics* **2013**, *32*, 6148.

[32] M. Kuriyama, R. Shimazawa, R. Shirai, *Tetrahedron* **2007**, *63*, 9393.

[33] H.-J. Huang, W.-C. Lee, G. P. A. Yap, T.-G. Ong, *J. Organomet. Chem.* **2014**, *761*, 64.

[34] a) A. Mariconda, M. Sirignano, C. Costabile, P. Longo, *Mol. Catal.* **2020**, *480*, 110570; b) C. Costabile, A. Mariconda, M. Sirignano, A. Crispini, F. Scarpelli, P. Longo, *New J. Chem.* **2021**, *45*, 18509; c) M. Sirignano, A. D'Amato, C. Costabile, A. Mariconda, A. Crispini, F. Scarpelli, P. Longo, *Front. Chem.* **2023**, *11*, 1260726; d) M. Sirignano, C. Costabile, A. Mariconda, P. Longo, *Results Chem.* **2023**, *6*, 101198; e) D. Iacopetta, C. Costabile, M. La Chimia, A. Mariconda, J. Ceramella, D. Scumaci, A. Catalano, C. Rosano, G. Cuda, M. S. Sinicropi, P. Longo, *ACS Med. Chem. Lett.* **2023**, *14*, 1567.

[35] A. J. Bridgeman, G. Cavigliasso, L. R. Ireland, J. Rothery, *J. Chem. Soc., Dalton Trans.* **2001**, *14*, 2095.

Manuscript received: August 9, 2024
Accepted manuscript online: September 16, 2024
Version of record online: November 5, 2024